Received 27 February 2024; accepted 19 March 2024. Date of publication 28 March 2024; date of current version 17 April 2024.

Digital Object Identifier 10.1109/OJCOMS.2024.3381978

Design and Implementation of a 5G NR Transmitter With Wi-Fi Coexistence by Beamforming and Power Control

YU-HAO LIU[1,2], CHENG-PANG KU[1], AND TZI-DAR CHIUEH[1] (Fellow, IEEE)

[1]Graduate Institute of Electronics Engineering, National Taiwan University, Taipei 10617, Taiwan

[2]Wireless Communication Technology, Mediatek Inc., Hsinchu 30000, Taiwan

CORRESPONDING AUTHOR: T.-D. CHIUEH (e-mail: chiueh@ntu.edu.tw).

This work was supported by the National Science and Technology Council of Taiwan under Grant MOST 110-2221-E-002-062-MY2.

ABSTRACT Telecom operators are under pressure to provide more spectrum resources to meet the increasing demand for high-throughput mobile communications. To achieve this, they have focused on unlicensed frequency bands, but the coexistence of 5G signals with other communication systems on these bands poses a challenge. To address this, beamforming technology has been introduced to reduce interference in space and enable independent demodulation of 5G and Wi-Fi signals. This paper implements a 5G base station (BS) prototype with an eight-antenna beamforming hardware transmitter, which concentrates the transmitted energy on individual 5G receivers while reducing the signal's impact on Wi-Fi receivers. Angle of arrival estimation and power control mechanisms are also integrated to enhance the efficiency of the solution. To verify the system coexistence, software-defined radio is used to realize 5G and Wi-Fi receivers. The proposed solution is demonstrated via over-the-air experiments to perform reliable transmission to multiple 5G receivers without interrupting Wi-Fi traffic on the same frequency band. The beamformer can also adjust its spatial profile and power level through environment-sensing functions built into the BS prototype. The proposed power control method delivers improved 5G transmitter and Wi-Fi transmitter energy performance by 50% and 51%, respectively.

INDEX TERMS 5G NR, WiFi, coexistence, over-the-air validation.

I. INTRODUCTION

WITH the continuous breakthrough of communication technology and the popularity of smart devices, users are increasingly concerned about user experience and data throughput. In addition to voice and audio-visual communication and entertainment needs, machine-based services such as the Internet of Things (IoT), self-driving cars, smart buildings, and smart cities are proliferating rapidly. These wireless networking applications require high-throughput mobile broadband services. To meet the challenge of the surge in such mobile data traffic, service providers worldwide are scrambling to license more spectrum and improve the spectrum efficiency of their services. Pushing their mobile services to the unlicensed spectrum is undoubtedly quite tempting and on their roadmaps.

In April 2020, the U.S. Federal Communications Commission (FCC) announced that a new 1200-MHz unlicensed frequency band is available for Wi-Fi 6 and other unlicensed wireless services. With this new unlicensed band, the coexistence of the 5G NR devices with other wireless devices in this band becomes a popular research topic. The benefits of coexistence in unlicensed bands are several, e.g., increased spectrum efficiency, lower deployment cost, and enhanced mobile connectivity. However, coexistence in unlicensed bands also poses challenges, such as the need for effective interference mitigation and coordination for fair spectrum sharing. Therefore, effective management of coexistence is critical to ensuring that the benefits of unlicensed spectrum coexistence are fully realized.

© 2024 The Authors. This work is licensed under a Creative Commons Attribution-NonCommercial-NoDerivatives 4.0 License.
For more information, see https://creativecommons.org/licenses/by-nc-nd/4.0/

The coexistence concept dates back to the 4G LTE era when many research efforts attempted to utilize unlicensed spectrum resources without disrupting existing WiFi and Bluetooth services. To manage the co-channel interference (CCI) of cellular and Wi-Fi technologies, Licensed Assisted Access (LAA) and LTE-U are the two most popular solutions. LAA adopts the Listen before talk (LBT) mechanism, where a device conducts "clear channel assessment" (CCA) to check whether the channel is occupied before its actual transmission [1], [2].

LTE-U mainly uses carrier sensing adaptive transmission (CSAT) technology, which does not require channel sensing [3] before transmission. In CSAT, cellular base stations (BSs) allot regular idle intervals in the transmitted waveforms and allow Wi-Fi devices to access the channel during those intervals [4]. Another technology, called MulteFire, does not require any licensed spectrum assistance and is similar to the LAA technology except for its ability to operate without existing licensed-spectrum networks [5]. In 5G NR, LTE-LAA evolves into *Anchored NR-U*, and MulteFire evolves into *Standalone NR-U*. Due to the higher licensing fee of the 5G spectrum, standalone NR-U that can operate independently and deploy quickly becomes more attractive.

In order to deploy 5G NR traffic on unlicensed bands, spectrum sharing between 5G NR signals and the prevalent WiFi signals is necessary. However, the current mainstream solutions, CSAT and LBT [6], [7], are both based on discontinuous transmission. The authors in [6] proposed a coexistence approach by leveraging LBT procedure for 5G NR-U devices and DCF procedure for WiFi devices. In [7], the authors exploited the bandwidth part (BWP) assignment technology to provide more opportunities for 5G operators to transmit in the unlicensed band using the LBT scheme.

The above approaches do not allow BSs and Wi-Fi access points (APs) to use unlicensed spectrum at the same time, leading to less efficient spectrum usage. Toward this end, many researchers tried to enhance spectrum efficiency by leveraging coexistence in the spatial dimension [8], [9], [10], [11], [12]. Beamforming is a directional transmission technology that can significantly improve system spectral efficiency and achieve interference-mitigated transmission in coexisting networks. Beamforming can enable 5G NR BSs and Wi-Fi APs to operate concurrently in unlicensed bands, thanks to its interference mitigation property. However, in [10], the authors applied different beamforming schemes, MRT or ZF, and the adopted scheme switches between MRT and ZF depending on the traffic load of WiFi, which cannot be sensed effectively. Another work relies on fixed spatial decomposing as well as the LBT technique to achieve the objective of maximizing the cellular system throughput [11]. However, the proposed scheme cannot cope with the case when UEs and STAs are mobile. Li and Liu [12] proposed a fixed DFT (Discrete Fourier Transformation) codebook for beamforming vectors and applied resource allocation and power control to mitigate the interference to WiFi devices. However, the DFT codebook and beam selection are not flexible enough to deal with complex scenarios in two coexisting mobile communication systems.

This paper proposes leveraging the beamforming technology at the 5G NR base station to spatially separate different user signals and reduce the interference on the receivers of another network (Wi-Fi). The proposed solution can effectively improve the SINR of the 5G and Wi-Fi receivers and enhance the overall spectral efficiency of the two coexisting wireless systems. We have improved the existing MVDR algorithm [13], [14] by adopting a window function to optimize the spatial filtering characteristics. This approach can more effectively suppress signal energy in non-target directions, thus achieving better coexistence of 5G and Wi-Fi transmissions in the same frequency band. In addition to utilizing downlink beamforming technology to transmit signals to 5G UEs and reduce interference on Wi-Fi STAs, we have also developed tracking of the coexisting devices via uplink signals. Toward this end, the 5G BS estimates the arrival angle of the coexisting device and recalculates the downlink beamforming coefficients accordingly. It then performs beam nulling based on the updated coexisting device's azimuth angle to suppress the interference inflicted on the Wi-Fi receivers. As a result, Wi-Fi STAs can continue to enjoy normal reception as they move around. Besides deploying the beamforming technology to improve the SINR of coexisting 5G and WiFi receivers, we also proposed a transmission power control scheme to increase the overall spectrum usage and transmission energy performance. Power control according to real-time sensing of transmission outcomes can optimize the SINR of all the receivers and attain reliable transmission for both systems.

To showcase the feasibility of our proposed coexistence transmission solution, we chose the Xilinx RFSoC as the wireless development platform for the 5G BS due to its cost-effectiveness and high flexibility. There are quite a few previous works on the prototype implementations exhibiting the LTE and 5G NR systems coexisting with WiFi traffic, such as [10], [15], [16], [17], [18], [19]. Among them, [10], [15], [16], [17] were for LTE and applied either the MRT/ZF beamforming scheme, the LBT scheme, or a time-domain interference cancellation (TDIC) solution. The works in [18] and [19] demonstrated the actual coexistence of the 5G NR system with the WiFi system. However, both of them implemented the LBT scheme in their prototypes. Our study presents a prototype for 5G-WiFi coexistence that eliminates the LBT mechanism and adopts beamforming-based space-division multiple access. In addition, this prototype, based on a cost-effective RFSoC FPGA platform, supports *device tracking* and *adaptive power control*.

Several next-generation wireless transmission prototypes, such as massive MIMO transmitters, employed the software-defined radio USRP devices provided by National Instruments ([20], [21], [22]). Each such device supports only two RF channels and two antennas. Therefore, each previous testbed required more than 60 such modules, incurring significant expenses in financial resources and

physical space. In this work, we adopted the Xilinx RFSoC as the wireless development platform for the 5G BS due to its cost-effectiveness and high flexibility. In the coexistence prototype, we adopted two Xilinx RFSoC platforms, each supporting up to eight RF input/output ports for simultaneous signal reception/transmission through multiple antennas. We designed and implemented an eight-antenna multi-user beamforming OFDM transmitter circuit, following the 5G NR R15 specification. To demonstrate the reliable transmission of two coexisting networks, we adopted multiple-antenna receivers for two UEs and single-antenna receivers for two STAs. Additionally, we developed another set of TX/RX for WiFi uplink transmission, which enables tracking of the WiFi STA's movement.

The main contributions of this paper are summarized as follows:

- Design a 5G NR transmitter system employing MVDR beamforming with windowing to guarantee smooth coexistence with WiFi traffic.
- Develop a 5G NR base station system tracking WiFi stations via MUSIC angle-of-arrival sensing in the uplink signal, integrating a novel power control mechanism monitoring the success rates of 5G and WiFi transmissions.
- Build a 5G NR BS prototype using the RFSoC FPGA and direct RF technology, featuring adaptive beamforming, device tracking, power control, and the capability to sense WiFi and UE signals.
- Conduct over-the-air (OTA) experiments to validate the transmission reliability and energy performance of the coexisting wireless standards using the proposed 5G BS prototype and real-time implementations of 5G UEs and WiFi AP/STA.

The rest of this paper is organized as follows. Section II introduces the basic principles of beamforming and the MVDR algorithm. Section III explains how to design device tracking and transmitter power control. Section IV describes the circuit and system architecture of the proposed 5G BS prototype consisting of an eight-antenna beamforming transmitter, a four-antenna receiver for the angle of arrival estimation, two multiple-antenna UE receives, WiFi software-defined transmitters/receivers, and a host PC controller that performs device tracking and power control functions. In Section V, we present the OTA experimental results of the 5G BS prototype that coexists with multiple WiFi transmission links in the same frequency band. Finally, Section VI provides the conclusion of this paper.

Notations: Uppercase boldface, lowercase boldface, and italic letters denote matrices, vectors, and scalars, respectively. $(\cdot)^T$ denotes transpose; $(\cdot)^H$ denotes transpose and complex conjugate. Uppercase boldface and uppercase italic letters denote sets with elements being vectors and scalars, respectively. $\|a\|$ stands for the magnitude of complex number a. $E\{\cdot\}$ denotes the expectation operator.

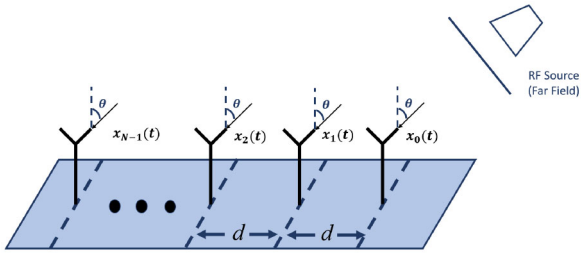

FIGURE 1. Illustration of far-field reception by an *N*-element antenna array with separation *d*.

II. OVERVIEW OF BEAMFORMING AND MVDR ALGORITHM

A. BEAMFORMING

Beamforming can be regarded as a filter in space. Generally, beamforming implementation involves an antenna array arranged in a specific way, such as the uniform linear array (ULA) or the uniform rectangular array (URA). Simplistic beamforming adjusts the phase differences between the signals feeding the antennas so that the signals form constructive interference along a specific angle, enhancing the energy transmitted in that direction. Destructive interference can also be formed along another angle(s) to reduce signal energy directed along that direction(s). Beamforming can be used not only at the transmitting side but also at the receiving side to increase the signal to interference and noise ratio (SINR) of the receive beamformer output.

Throughout this paper, we will adopt a ULA for transmitter beamforming. In a ULA, N identical isotropic sensors are placed at equal intervals d on a straight line. Moreover, we also assume that the distance d_F between the receiver and the antenna array satisfies the far-field criterion,

$$d_F > 2D^2/\lambda, \tag{1}$$

where D is the radius of the antenna, and λ denotes the wavelength of the transmitter signal's carrier frequency. With this condition, the receiver is at a far-field position and the signals entering the receiver antenna elements are assumed parallel, as shown in Figure 1.

When the incident signal is a parallel wave, each antenna will experience a time delay in receiving the signal. When the signal received by the antenna is a narrowband signal, the time difference of the signal received by the antenna can be converted into a phase difference. Receive beamforming adjusts the phase difference between signals from the antennas to align these signals and achieve constructive interference. A basic beamforming method uses a steering vector as the beamforming coefficients, so that the main lobe (strongest signal direction) points in a specific direction in space. A steering vector takes the form of

$$\mathbf{a}(\theta_0) = \left[1 \; e^{-j\pi \sin(\theta_0)} \; e^{-j2\pi \sin(\theta_0)} \cdots e^{-j(N-1)\pi \sin(\theta_0)}\right]^T, \tag{2}$$

where θ_0 is the main lobe direction.

B. MVDR ALGORITHM

Minimum-Variance Distortionless Response (MVDR) is another beamforming algorithm [8], [9], which is mainly used at the receiving end to suppress signals from sources in a specific direction through spatial feature analysis. The MVDR algorithm calculates the beamforming coefficient vector $\mathbf{w}$ based on the following two requirements. The first is to make the beamformed signal in the direction from the target not be distorted, so the signal energy in the direction of the target must be 0 dB, i.e.,

$$\mathbf{w}^H \mathbf{a}(\theta_0) = 1. \tag{3}$$

The second requirement is to minimize the total energy of the beamformed signal so as to minimize the noise in the beamformer output. The total beamformed signal energy is given by

$$E\{|y|^2\} = E\{|\mathbf{w}^H \cdot \mathbf{x}|^2\} = \mathbf{w}^H \hat{\mathbf{R}}_{\mathbf{xx}} \mathbf{w}, \tag{4}$$

where $\hat{\mathbf{R}}_{\mathbf{xx}}$ denotes the sample covariance matrix of the beamformer input signal and

$$\hat{\mathbf{R}}_{\mathbf{xx}} = \frac{1}{K} \sum_{k=1}^{K} \mathbf{x}(k) \mathbf{x}^H(k). \tag{5}$$

The MVDR algorithm is formulated as the following constraint optimization problem.

$$\min_{\mathbf{w}} \mathbf{w}^H \hat{\mathbf{R}}_{\mathbf{xx}} \mathbf{w}, \quad \text{s.t.} \ \ \mathbf{w}^H \mathbf{a}(\theta_0) = 1. \tag{6}$$

Through the Largrange method, the solution to the MVDR algorithm is given by

$$\mathbf{w}_{\text{MVDR}} = \frac{\mathbf{R}_{\mathbf{xx}}^{-1} \, \mathbf{a}(\theta_0)}{\mathbf{a}^H(\theta_0) \, \mathbf{R}_{\mathbf{xx}}^{-1} \, \mathbf{a}(\theta_0)}. \tag{7}$$

Note that the MVDR algorithm can also be applied at the transmitter side through appropriate reformulation. For the transmitting MVDR beamformer, the covariance matrix $\hat{\mathbf{R}}_{\mathbf{xx}}$ does not exist, therefore it is replaced by the summation of transmitting signal vectors' outer product matrix given by

$$\mathbf{R}_{\mathbf{xx}} = \mathbf{a}(\theta_0) \, \mathbf{a}^H(\theta_0) + \sum_{i=1}^{I} \mathbf{a}(\theta_i) \, \mathbf{a}^H(\theta_i) \ + \ \sigma_n^2 I, \tag{8}$$

where $\mathbf{a}(\theta_0)$ is the steering vector of the beamforming target at angle θ_0, and $\mathbf{a}(\theta_i)$ is the steering vector of the nulling angle θ_i. Note that a regularization term that accounts for the noise term is included.

A typical beam pattern of an MVDR beamformer is illustrated in Figure 2, where the horizontal axis is the angle in space, and the vertical axis represents the signal power. The angle with the highest signal energy is called the *main lobe*, and the angles with almost no signal power are called the null points. In this figure, an 8-antenna uniform linear array (ULA) is simulated with the main lobe angle being $+20°$ and three null points at $-30°$, $+0°$, and $+60°$. The simulated beam pattern shows that the target angle has the highest signal power, while the power at the null point directions is almost zero.

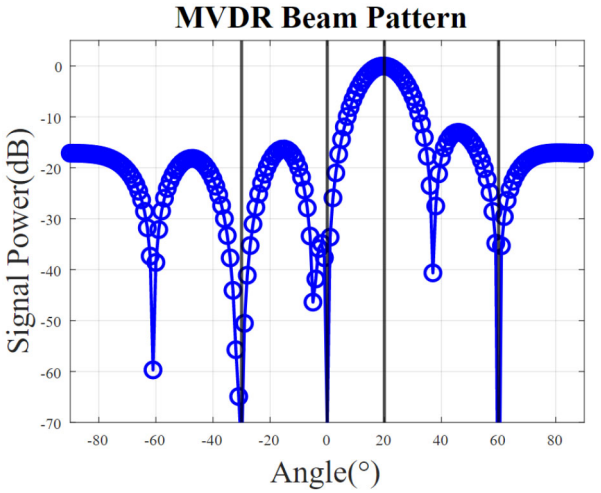

FIGURE 2. Beam pattern of the MVDR beamformer (beam direction: $+20°$, null points: $-30°$, $+0°$, and $+60°$).

III. DEVICE TRACKING AND POWER CONTROL

The aforementioned MVDR beamformer makes the assumption that the azimuth angles of both the 5G UE and Wi-Fi STA are stationary and known. However, in reality, the positions of receivers are often not fixed, and they tend to move with the users. Consequently, the 5G BS does not know the Wi-Fi STA's azimuth angle, leading to theoretical limitation. To overcome this, we implemented the angle of arrival (AoA) estimation based on the Wi-Fi STA's uplink signal. This enhancement enables the tracking of the Wi-Fi STA device even when it is on the move and its position is not fixed. With this upgrade, the 5G BS can track the Wi-Fi STA's location, and the 5G BS downlink transmitter can update its beamformer coefficients and efficiently transmit data to the UEs, providing a seamless and uninterrupted user experience. Moreover, it is worth noting that the current design focuses on tracking coexisting devices (Wi-Fi STAs) rather than tracking UEs in the 5G network. However, the same methodology can also be applied to track the 5G UEs.

The 5G beamforming transmitter has fixed power levels for signals intended for UEs, which can lead to improper interference levels inflicted on the coexisting Wi-Fi transmission. Dynamic power control technology is critical for the 5G BS to manage these challenges. As both Wi-Fi and 5G systems send acknowledgments after downlink transmission to indicate successful reception and decoding, the 5G BS can monitor the success rate of both systems and dynamically adjust the output power of the 5G downlink transmitter.

A. COEXISTENCE DEVICE TRACKING

The proposed 5G BS employs the MUSIC (MUltiple SIgnal Classification) algorithm [23], [24] to estimate the azimuth angle of the WiFi STA signal. The MUSIC algorithm begins by calculating the covariance matrix of the received signals from the antenna array. The covariance matrix is then decomposed to obtain the signal subspace (from WiFi STA)

and the noise subspace. These subspaces are orthogonal to each other and are used to construct the spatial spectrum. The angle of arrival for the WiFi STA is determined by identifying the peaks in the spatial spectrum.

In a receiver with N antennas, assume that the received signal comprises M signal sources and noises. The received signal vector $\mathbf{x}$ is formulated as

$$\begin{aligned}\mathbf{x} &= \sum_{i=1}^{M} \mathbf{a}(\theta_i)s_i + \mathbf{n} \\ &= \mathbf{As} + \mathbf{n},\end{aligned} \tag{9}$$

where $\mathbf{A}$ and $\mathbf{s}$ denote the matrix consisting of steering vectors and the transmitted signal vectors of the M signal sources, respectively, and $\mathbf{n}$ is the noise vector. The covariance matrix can be estimated by

$$\begin{aligned}\mathbf{R_{xx}} &= E\{(\mathbf{As}+\mathbf{n})\ (\mathbf{As}+\mathbf{n})^H\} \\ &= \mathbf{A}E\{\mathbf{ss}^H\}\mathbf{A}^H + E\{\mathbf{nn}^H\} \\ &= \mathbf{AR_{ss}A}^H + \sigma_n^2\mathbf{I},\end{aligned} \tag{10}$$

where $\mathbf{R_{ss}}$ is the covariance matrix of the M transmitted signals, σ_n^2 is the noise power, and $\mathbf{I}$ is the identity matrix.

Next, the covariance matrix $\mathbf{R_{xx}}$ undergoes eigenvalue decomposition, which results in N eigenvalues and N eigenvectors. Among them, the M eigenvectors $\mathrm{v}_1, \mathrm{v}_2, \ldots, \mathrm{v}_M$ with larger eigenvalues represent the M-dimensional signal subspace, while the remaining $N-M$ eigenvectors constitute the noise subspace. The signal subspace and the noise subspace are orthogonal to each other, and the noise subspace is given by

$$\mathbf{E}_n = \left[\mathbf{v}_{M+1},\ \mathbf{v}_{M+2},\ \ldots\ \mathbf{v}_N\right] \tag{11}$$

By the orthogonal property of the signal subspace and the noise subspace, we can evaluate the spatial spectrum according to.

$$P_{\mathrm{MUSIC}}(\theta) = \frac{1}{\mathbf{a}^H(\theta)\mathbf{E_n}\mathbf{E_n}^H\mathbf{a}(\theta)} \tag{12}$$

Finally, the angle of arrival is found by identifying the peaks in the spatial spectrum. Since there may be multiple signal sources in the space, the spatial spectrum may have multiple peaks.

B. POWER CONTROL

The proposed power control mechanism dynamically adjusts the output power of the 5G BS transmitter based on the success rates of the 5G UE receivers and the Wi-Fi STA receivers. The 5G NR R15 standard requires the 5G UEs to provide feedback through Hybrid Automatic Repeat Request acknowledgment (HARQ-ACK) to inform the 5G BS of the successful decoding of the downlink transmission. Similarly, the Wi-Fi 6 standard specifies that the Wi-Fi STA sends an ACK packet to inform the Wi-Fi AP of the successful reception and decoding of a packet. By monitoring the HARQ-ACK from the 5G UE and detecting the ACK from the Wi-Fi STA, the 5G BS can calculate the transmission success rates of the receivers in two systems and adjusts the 5G BS downlink transmission power accordingly. To detect the ACK returned by the Wi-Fi STA, the 5G BS is equipped with Wi-Fi reception capability.

To monitor the transmission success rates of both systems, we maintain separate 5G and Wi-Fi response queues that store the past R transmission outcomes. When the 5G UE successfully decodes a downlink signal, we append a "1" to the end of the 5G queue. Otherwise, we append a "0". Similarly, when the Wi-Fi STA successfully receives and decodes a downlink signal, we add a "1" to the end of the Wi-Fi queue; otherwise, we add a "0". The oldest outcome is discarded each time a new one is added, so each queue always records the most recent R outcomes.

Using the information in these queues, we propose a history-based power control method that outperforms the simple fixed-step method [25]. The 5G BS dynamically adjusts its transmission power level based on the success rates of the UE and STA receivers. Specifically, we define α and β as the success rates of the Wi-Fi STA and 5G UE receivers, respectively, over the past R transmission outcomes. The 5G BS transmitter power level (P_{BS}) is then adjusted as follows:

$$\Delta P_{BS} = \begin{cases} \delta \cdot P_{BS} & \text{if } \alpha > \lambda_H \text{ and } \alpha \uparrow \text{ and } \beta < \lambda_L \\ -\delta \cdot P_{BS} & \text{if } \alpha < \lambda_L \text{ and } \alpha \downarrow \\ 0 & \text{otherwise} \end{cases} \tag{13}$$

where δ is the adjustment ratio, λ_H and λ_L are the system parameters that specify the upper and lower limits of the receiver success rates, respectively. By adapting the transmission power level based on the success rates of both receivers, our proposed mechanism aims to maximize the overall transmission success rate and improve the quality of service for users in both systems.

IV. 5G NR BASE STATION PROTOTYPE COEXISTING WITH WIFI

We have developed a 5G NR BS prototype with coexistence device tracking and power control by utilizing two Xilinx RFSoC evaluation platforms and a host PC. The first Xilinx RFSoC platform acts as a 5G 8-antenna transmitter, using the beamforming technology to transmit signals to the 5G UEs while minimizing interference to the Wi-Fi STAs. The second Xilinx RFSoC platform implements a 4-antenna receiver for receiving the uplink signal from the Wi-Fi STA and it forwards the signal to the host PC for AoA estimation and power control. Notably, the Wi-Fi STA uplink signals are transmitted through an over-the-air (OTA) channel, while the 5G UE uplink HARQ-ACK signals are transmitted through Ethernet.

A. EIGHT-ANTENNA 5G NR BEAMFORMING TRANSMITTER DESIGN

Table 1 lists the parameters related to the 5G NR R15 BS downlink transmitter. In this design, the transmission

TABLE 1. 5G NR R15 downlink transmitter parameters.

Parameter	Setting
Carrier Frequency	2.55 GHz
Baseband Sample Rate	61.44 MHz
Transmission Bandwidth	40 MHz
CP Type	Normal CP
Subcarrier Spacing	15 kHz
FFT Size	4096
Used Subcarrier	2592
Modulation Order	QPSK, 16QAM
Code Rate	2/3, 1/2, 2/5, 1/3, 1/5
Lifting Size	8, 16, 32, 64, 128

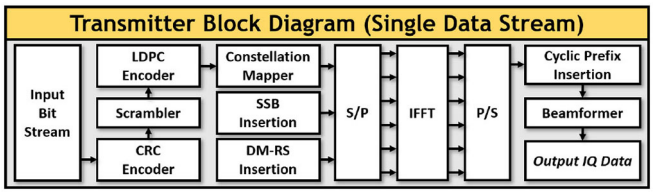

FIGURE 3. Architecture of the baseband OFDM transmitter with beamforming capability.

bandwidth is set to 40 MHz with a subcarrier spacing of 15 kHz and the FFT size is 4096. Moreover, the baseband sampling rate is set to 61.44 MSample/s. Among the 4096 subcarriers, a total of 2592 subcarriers are used, and the remaining 1504 subcarriers are used as guard bands. The data modulations implemented in this work are QPSK and 16QAM. The forward error correction (FEC) code used is QC-LDPC code and the transmitter supports five code rates and five lifting sizes. In addition, we applied the aforementioned MVDR beamforming algorithm plus some windowing to improve the spatial filtering characteristics, and specifically reduced power levels along non-target angles.

1) DESIGN OF THE BASEBAND OFDM TRANSMITTER WITH BEAMFORMING

The architecture of the baseband OFDM transmitter circuit with beamforming is shown in Figure 3. The circuit consists of two major blocks. The first block is the outer transmitter that implements bit-level processing, and it includes a CRC encoder, scrambler, and LDPC encoder. The second block is the inner transmitter that generates the in-phase and quadrature-phase (I/Q) baseband signals for the RF upconverter. This block implements constellation mapping, SSB (Synchronization Signal Block) insertion, DM-RS (Demodulation Reference Signal) insertion, IFFT, cyclic prefix insertion, and beamformer.

In the outer transmitter design, we referred to CRC-24B [26] in the 5G NR specification for the CRC encoder and adopted the fast-parallel CRC encoder design proposed in [27]. The scrambler scrambles the user's transmission data with pseudo-random binary sequences defined in the 5G NR specification [28]. Finally, the LDPC encoder is realized using the Xilinx Soft-Decision Forward Error Correction (SD-FEC) IP [29], which supports LDPC Encode/Decode for 5G NR with multiple code rates.

The constellation mapper performs binary-bit-to-symbol-IQ conversion, supporting QPSK and 16QAM. The SSB and DM-RS, which facilitates synchronization and channel estimation in the receiver, are inserted in the IQ signal sample sequences. The IFFT IP provided by Xilinx is employed to convert the frequency-domain IQ signals on the subcarriers to the time-domain IQ signals. The beamformer consists of eight complex-value multipliers that multiply the baseband time-domain I/Q samples with the beamforming coefficients to achieve beamforming in space.

2) INTEGRATION OF XILINX RFSOC PLATFORM AND THE BASEBAND TRANSMITTER

The Xilinx RFSoC platform consists of a main development board, the ZCU111 evaluation board, and a radio frequency (RF) daughterboard, XM500 RFMC Balun add-in card. The main System on Chip (SoC) FPGA chip integrates a Processing System (PS) with two ARM CPUs, a Programmable Logic (PL), and RF Data Converter IP (RFDC IP). The PL side comprises field-programmable logic elements and interconnection fabric for reconfigurable circuit implementation. The RFDC IP is responsible for converting baseband time-domain IQ signals to RF signals or RF signals to baseband signals. Xilinx RFSoC uses the direct conversion structure, which has advantages such as smaller size and more power efficiency compared to the traditional heterodyne RF structure. The RFDC IP in Xilinx RFSoC supports up to 8 sets of RF-DACs with a maximum sampling rate of 6.554Gsample/s and eight sets of RF-ADCs with a maximum sampling rate of 4.096 GSample/s. In this wireless transmitter integration, the XM500 RFMC Balun add-in card receives analog signals generated by the RF-DACs on the main board through a high-speed transmission interface, connects to antennas through SMA cables, and transmits the RF signals.

The proposed 5G NR R15 downlink transmission system architecture is depicted in Figure 4. The baseband transmitter supports up to four data streams and achieves multi-user transmission (MU-MIMO) with four beamforming transmitters, denoted as HW Tx1 through HW Tx4. In addition to Xilinx RFSoC, this transmission system requires a host PC as a controller, which handles data transfer and controls various parameters in the transmission system, such as modulation order, LDPC code rate, etc.

The transmission process is as follows: the host PC will send binary user data and pre-calculated downlink beamforming coefficients to the PS-side memory via Ethernet. Then, the host PC will trigger Xilinx AXI4-Lite and Xilinx CDC Macro to write the beamforming coefficients into the beamformer module of the baseband transmitter, as indicated by the red arrows in Figure 4. Afterwards, the host PC will trigger Xilinx DMA IP to quickly move the user data to the PL side, as indicated by the blue arrows

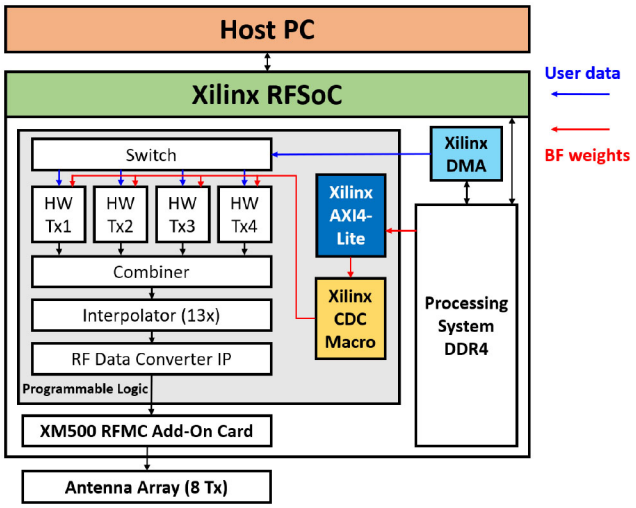

FIGURE 4. System architecture of the eight-antenna 5G NR RF transmitter platform.

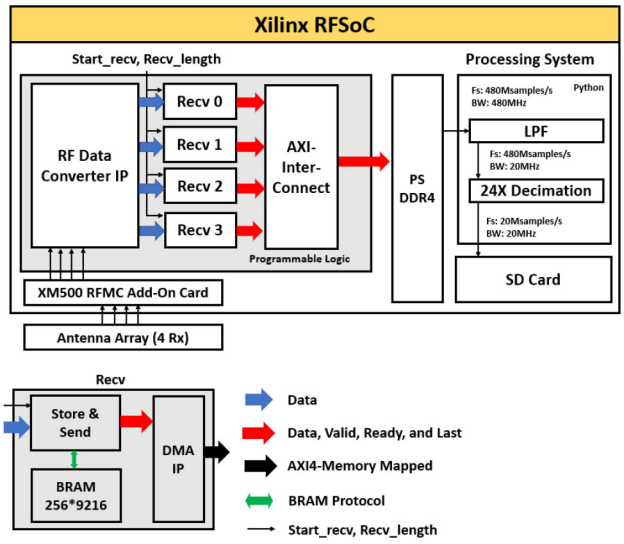

FIGURE 5. System architecture of the four-antenna WiFi receiver platform.

in Figure 4. The switch module allocates data streams to the corresponding beamforming OFDM Tx circuits, which convert user data into time-domain I/Q waveforms sampled at 61.44 Msample/s. These waveforms are then summed together through the combiner module. The combined time-domain signal is then up-sampled to 798.72 Msample/s using a time-domain interpolator circuit. Finally, the samples are sent to the RFDC IP for conversion to RF waveform, completing the baseband signal processing.

Then, the RF signal is transmitted to the Tx antenna array via the high-speed transmission interface, connected to the XM500 RFMC Balun add-in card. The RFDC IP adopts the direct-conversion technique with a DAC sampling rate of 6389.76 Msample/s. The RFDC IP's internal interpolator allows only up to 8x upsampling. Therefore, the baseband signal goes through two upsampling stages: the first from 61.44 Msample/s to 798.72 Msample/s, and the second from 798.72 Msample/s to 6389.76 Msample/s. Note the TX antenna separation in the BS prototype is half of the carrier wavelength and is set to 5.88cm.

B. FOUR-ANTENNA WIFI RECEIVER DESIGN

This section will describe the architecture and implementation of the four-antenna WiFi receiver for coexistence device tracking and power control. In principle, the frequency for the WiFi uplink (STA to AP) should ideally match the downlink frequency. Nevertheless, due to the constraint posed by the maximum sampling rate of Xilinx RFSoC's RF-ADCs at 4.096 Gsample/s, the WiFi uplink receiver implemented on an RFSoC platform is unable to support carrier frequencies higher than 2.048 GHz. Therefore, the carrier frequency of the WiFi uplink signal is set to 1.8 GHz. As such, the RX antenna separation is set to 8.33cm, also half of the carrier wavelength. To convert the RF signal with a carrier frequency of 1.8 GHz to a baseband signal with a sampling rate of 20 Msample/s, the RFDC IP parameters are set as follows: the RF-ADC sampling rate is set to 3.84 Gsample/s, the carrier frequency is set to 1.8 GHz, and the internal 8x decimator provided by the RFDC IP is used to down-sample the baseband signal to 480 Msample/s, reducing the throughput of the PL-PS data link. Figure 5 depicts the block diagram of the proposed receiver. Note that on the PL side there are four receive modules that buffered the down-converted baseband waveforms.

The four baseband signals generated by the RFDC IP of the four antennas are stored in the individual buffers of the four modules. Then, the DMA IP moves the four chunks of baseband signals from the PL side to the PS side. At this point, the signals are baseband signals with a sampling rate of 480 Msample/s. Since our ultimate goal is to obtain Wi-Fi baseband signals with a sampling rate of 20 Msample/s, additional filtering and 24x decimation are required on the PS side. With this, the signal processing on the Xilinx RFSoC receiver side is completed, and the four baseband waveforms received from the WiFi STA are stored in the SD card for further processing by the host PC.

C. PROTOTYPE INTEGRATION SOFTWARE

The 5G BS prototype consists of three main subsystems: Rx RFSoC, host PC, and Tx RFSoC. The three subsystems are connected by Ethernet for file exchange. The software functions of these subsystems are shown in Figure 6, and will be introduced below.

The Rx RFSoC's PS side runs a Python code that controls the associated PL side to perform four-antenna reception and then transfer the down-converted signals to the PS side. The code then performs filtering and 24x decimation on the signals and saves them as files on the SD card of the Rx RFSoC. Finally, using the Ncat software, a connection is established between Rx RFSoC and the host PC, and the received waveforms' files are transferred to the host PC. The Rx RFSoC repeats this procedure to provide the latest Wi-Fi uplink signals to the host PC for AoA estimation, beamforming design, and power control.

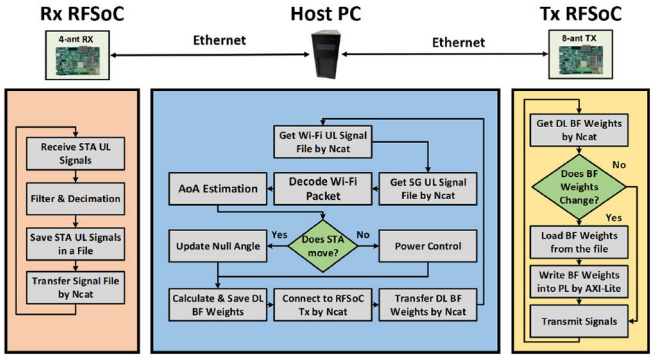

FIGURE 6. Software functionalities of the Rx RFSoC, host PC, and Tx RFSoC of the BS prototype.

The Tx RFSoC executes a Python code on the PS side that performs the following steps. At first, the program receives the downlink beamforming coefficients sent from the host PC and saves them to the SD card. Then, by comparing the newly received coefficients with the coefficients on file, the PS side program decides whether or not to transfer the updated coefficients to the beamformer module in the PL side using AXI4-Lite. Finally, the PS side triggers the PL side to transmit the beamformed RF signal with the current power level. Similar to the Rx RFSoC, the Tx RFSoC repeats these steps continuously to ensure that the 5G BS transmits 5G downlink signal with up-to-date beamforming coefficients and output power.

The host PC controls the entire 5G BS prototype using a MATLAB code, which also implements the WiFi software receiver packet decoding, the STA angle of arrival estimation, and the BS transmitter power control. Firstly, the host PC stores the data received from Rx RFSoC, then uses the MUSIC algorithm to perform AoA estimation and packet decoding on the WiFi uplink signal. Next, the host PC determines whether the WiFi STA has moved based on the difference between the current and previous angle of arrival estimates, with a threshold of 5 degrees. If the WiFi STA has moved, the null angle is updated, and the window-based MVDR beamforming coefficients are recalculated, followed by transferring the updated beamforming coefficients from the host PC to the Tx RFSoC. In addition, the history-based power control mechanism is performed. If the output power changes, the downlink beamforming coefficients are recalculated and transferred to Tx RFSoC. The host PC continuously performs these steps to ensure seamless service by the 5G BS prototype to the 5G UEs, while minimizing any interference with the WiFi traffic that may overlap with the 5G transmission.

D. RECEIVERS OF 5G UES AND WIFI STAS

To implement the four-antenna 5G UE receiver, we used NI USRP devices and a host PC. Since each 2943R USRP device has two Rx channels, we adopted two such USRP devices to construct the four-antenna receiver for UE 1. The devices used in this UE receiver and their architecture is depicted in Figure 7(a).

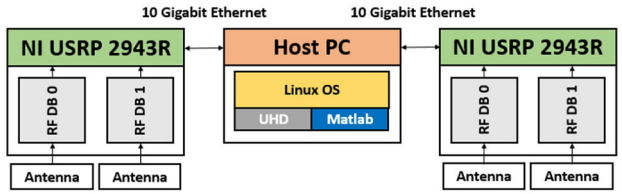

(a) Devices used in the four-antenna UE RX.

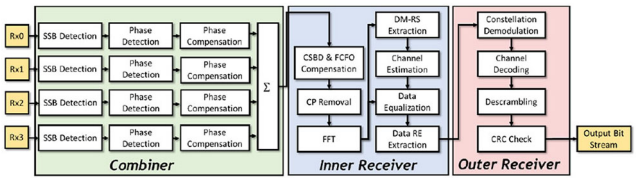

(b) Block diagram of the 5G UE baseband RX.

FIGURE 7. Four-antenna receiver of 5G NR UE.

TABLE 2. Parameters of 8-ant 5G NR Tx and Wi-Fi Tx.

Parameter	*NR-U setting*	*Wi-Fi 6 setting*
Antenna Number for BS Tx	8	1
Antenna Number for UE Rx	UE1 Rx: 4	1
	UE2 Rx: 2	-
Carrier Frequency	2.55 GHz	2.55 GHz
Baseband Sample Rate	61.44 MHz	20 MHz
Transmission Bandwidth	40 MHz	20 MHz
CP Type	Normal CP	-
Subcarrier Spacing	15 kHz	78.125 kHz
FFT Size	4096	256
Used Subcarrier	2592	242
Modulation Order	QPSK/16QAM	QPSK/16QAM
Code Rate	1/3	1/2

Inside the USRP, after receiving the RF signals through the antenna, it first goes through a low noise amplifier (LNA) and a driver amplifier to amplify the signal. The analog signal is then converted to a digital signal by an ADC, and is further processed by a digital down converter (DDC) to convert it to baseband. Finally, a digital filter is used for low-pass filtering, completing the signal processing on the receiving end. The processed signal is then transmitted to the Host PC via a 10 Gbit Ethernet cable. In the host PC, we use MATLAB to do software OFDM demodulation and FEC decoding. The decoding flow chart is in Figure 7(b).

Details of 5G UE 2 and Wi-Fi STAs are identical to the above description, except that UE 2 has only two antennas whereas all STAs have one antenna.

V. OTA EXPERIMENTS

This section will describe the verification of the proposed 5G and Wi-Fi coexistence system in an OTA environment. The first OTA experiment was to verify reliable data

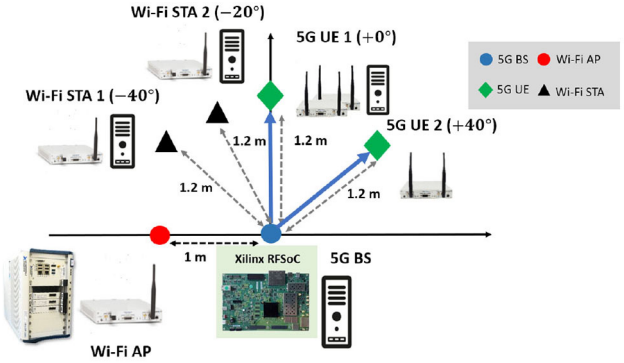

(a) Equipment setup.

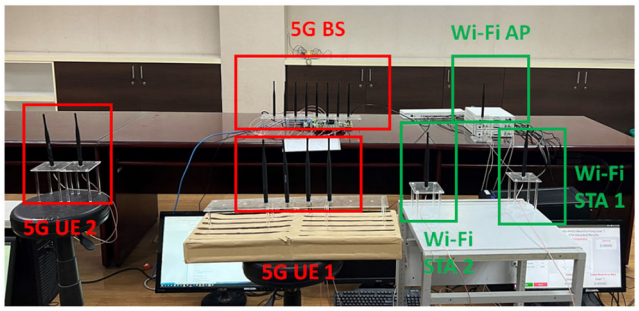

(b) Experiment environment.

FIGURE 8. Experiment setup of the 5G NR and WiFi coexistence trials.

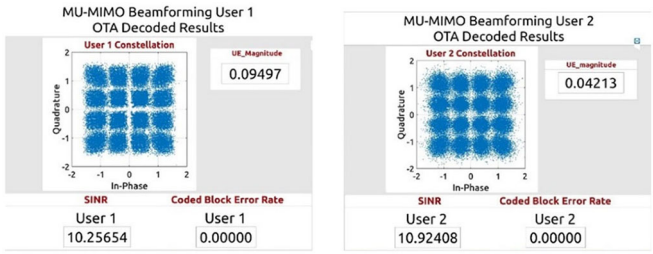

(a) UE1 Rx performance.

(b) UE2 Rx performance.

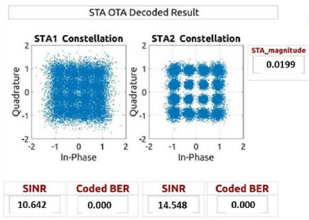

(c) STA1/STA2 Rx performance.

FIGURE 9. Receiver performance of the OTA coexistence experiment using 16QAM modulation. (a) UE1, (b) UE2, and (c) STA1/STA2.

transmission from a single 5G downlink BS transmitter to two multi-antenna UEs, while another WiFi access point (AP) transmitted data to two WiFi STAs. The second experiment implemented a more elaborate coexistence design that includes the estimation of the STA signal's arrival angle and the corresponding beamforming coefficient update, as well as the proposed history-based power control method. The final experiment compared our power control method with the traditional fixed-step power control method in an OTA trial to showcase the effectiveness of the proposed approach.

A. EIGHT-ANTENNA TRANSMITTER SUPPORTING 5G AND WIFI COEXISTENCE

This experiment is a real-time measurement of the performance of the 5G-WiFi coexistence system proposed in this paper through OTA channels. Table 2 lists the parameters used in the experiment, with an eight-antenna 5G BS transmitting signals and two 5G UEs using four and two antennas, respectively, to receive signals. The Wi-Fi AP and two Wi-Fi STAs all have a single antenna. Both 5G and Wi-Fi transmitters use OFDM technology with 16QAM modulation. 5G NR BS uses LDPC code with a code rate of 1/3, while Wi-Fi AP uses LDPC code with a code rate of 1/2. Finally, the 5G BS uses windowed MVDR beamforming technology for signal transmission, while the Wi-Fi AP uses a single antenna for transmission.

Figure 8(a) depicts the OTA experimental setup consisting of one 5G BS at the origin, one WiFi AP one meter to the left of the 5G BS. A four-antenna UE receiver is at 0°; another two-antenna UE is at +40°. The two single-antenna WiFi STAs are at −20° and −40°, respectively. All four receivers are 1.2 meters away from the 5G BS. A photograph showing the actual experimental environment is given in Fig. 8(b). Note that only the antennas are visible, instruments such as host PC, Xilinx RFSoC platform, and USRP SDR are not shown in the figure.

Figures 9(a), (b), and (c) depict screendumps exhibiting the decoding outcomes of 5G UE1, 5G UE2, Wi-Fi STA1/STA2, respectively. The results include received signal magnitude, constellations of equalized signals and their error-vector magnitude (EVM), and error rates of LDPC codewords. Despite the interference between the 5G and Wi-Fi transmitters and their respective receivers, the windowed MVDR beamforming technique successfully reduces these interferences. As a result, all four 5G/Wi-Fi receivers exhibit zero LDPC decoder error rates. This outcome illustrates the simultaneous and dependable transmission of both 5G and Wi-Fi systems. Additionally, our proposed beamformer-based approach enables coexistence without relying on less throughput-efficient interference avoidance methods, such as LBT.

B. WIFI DEVICE TRACKING AND POWER CONTROL

This experiment aims to verify two advanced features of the proposed solution: WiFi STA tracking and power control of the 5G BS transmitter. To allow a larger range of movement and tracking, we use only one UE and one STA in this experiment. The parameters used are listed in Table 2.

The scenario of the experiment is shown in Figure 10, while the environment is similar to that in Fig. 8(b). An

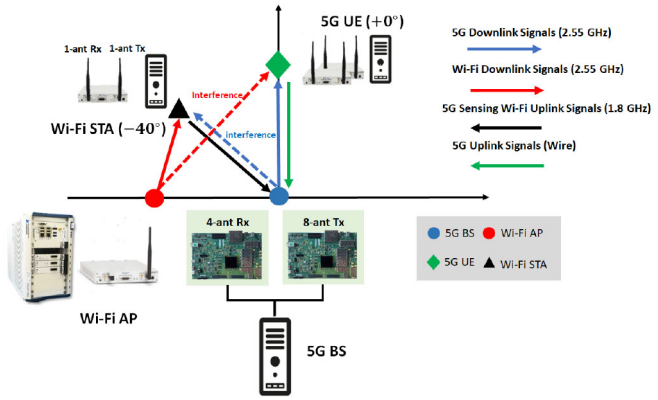

FIGURE 10. Experiment setup of the coexistence system with WiFi device tracking and power control.

extra Xilinx RFSoC platform is installed to work as a four-antenna WiFi receiver at the 5G BS, allowing it to continuously monitor the azimuth angle of the Wi-Fi STA. The 5G UE uses a four-antenna array for reception and is placed approximately 1.2 meters away from the 5G BS at $+0°$ angle. The Wi-Fi AP is placed at the same horizontal line as the 5G BS, about 1 meter away. The Wi-Fi STA is located 1.2 meters away from the 5G BS at $-40°$ angle. Power control is performed based on the detected ACK from the Wi-Fi STA, as well as the 5G UE's HARQ-ACK, which is fed back to the BS through a wired connection. The power control algorithm has several parameters and we set them to the following: response queue size $(R) = 20, \lambda_H = 0.95, \lambda_L = 0.8, \delta = 0.3$.

In summary, the BS designs beamforming coefficients according to the detected STA azimuth angle to reduce the interference of the 5G BS's signal on the Wi-Fi STA. The proposed power control method can dynamically adjust the 5G BS's transmission power to ensure a certain success rate for both the 5G and Wi-Fi systems, maintaining the coexistence of both systems. To demonstrate the capability of the 5G BS prototype to track the WiFi STA and adjust its beamforming accordingly, we have shot a video of a series of experiments. In this video, the WiFi STA is shown to move around and still achieve reliable reception without interference from the 5G BS. This video can be found at https://www.youtube.com/watch?v=DimTeFXqX1E

Next, we conducted experiments that illustrate how power control can properly allocate power to the 5G BS transmitter and ensure the coexistence of 5G and WiFi traffic. Figure 11 shows a screen snapshot of the two receivers' performance in this experiment, including transmitter power, success rate, EVM, equalized constellation, estimated STA arrival angle, etc. Note the MUSIC spatial spectrum in the upper left of the figure, which exhibits a peak at approximately $-40°$ that is consistent with the Wi-Fi STA location. At time index 40, the Wi-Fi AP transmission power was lowered by 10 dB, resulting in the Wi-Fi STA's constellation becoming quite blurry, and no ACK packet

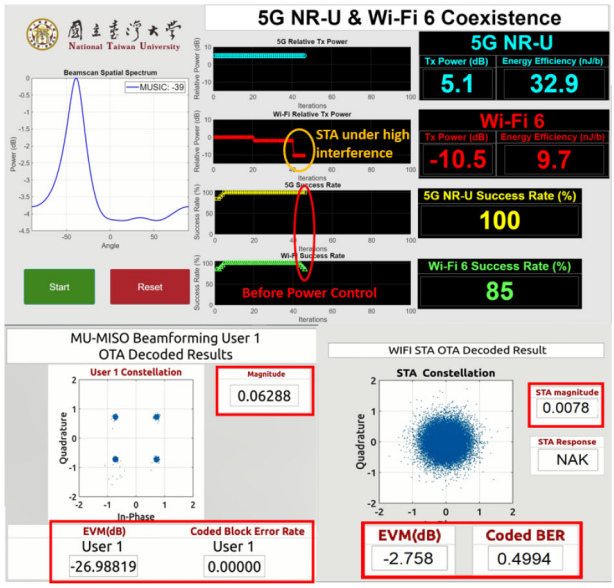

FIGURE 11. Transmission performance of the power-control coexistence experiment. AP Tx lowers power by 10dB and 5G BS Tx has no power control.

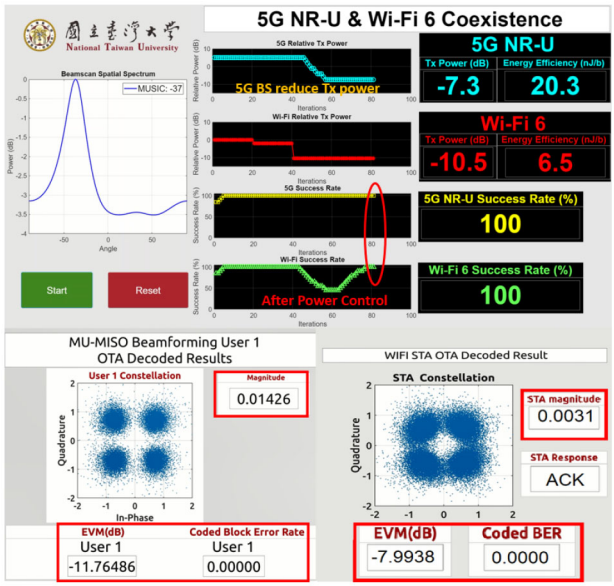

FIGURE 12. Transmission performance of the power-control coexistence experiment after power control has been turned on.

was detected by the 5G BS. Thus, the estimated Wi-Fi transmission success rate started to decline (the green curve).

When the Wi-Fi transmission success rate fell below the low threshold (λ_L), the 5G BS activated power control and adjusted its transmitter power. From Figure 12, it can be observed that after the power control kicks in, the 5G BS transmission power decreases from 5.1dB to -7.3dB. The WiFi QPSK constellation became more distinct than that in Fig. 11. Moreover, the STA receiver's coded BER was reduced to 0. Although the decrease in 5G BS Tx power made the 5G UE's received constellation slightly blurry, it still was capable of reliable transmission. Note that at

time index 80, both systems' transmission success rates went back to 100%. We have created another demonstration video of the OTA experiment showing the proposed 5G BS prototype implementing power control, which can be found at https://youtu.be/WBou0ze757g

C. PERFORMANCE COMPARISON OF POWER CONTROL METHODS

This experiment compared different power control methods in more detail. The system parameters and power control parameters are the same as before. The experimental setup and environment are as in Figure 10.

We ran the 5G BS prototype with different power control methods for 300 time steps each, when the Wi-Fi AP transmission power was tuned manually. As shown in Figure 13(a), the AP power (black curve) was first reduced by 2 dB at time index 20, and then reduced to -10 dB at time index 40. These power-level changes aimed at testing 5G BS power control mechanism in response to severe interference experienced by the Wi-Fi STA. Furthermore, at time index 200 the AP transmission power was increased by 10 dB. This change was intended to test the case when there was severe interference to the 5G UE.

It is clear from Figure 13(a) that the proposed history-based fixed-step power control method delivered a more stable 5G Tx power profile (green curve), while the Tx power profile controlled by the fixed-step power control method in [25] (red curve) oscillates erratically. The reason for this advantage is that the proposed method considers past success rates, thus avoiding too frequent power-level changes that may lead to unreliable transmission of 5G or Wi-Fi. Figures 13(b) and 13(c) depict the success rates of the 5G UE Rx and Wi-Fi STA Rx, respectively. The history-based power control method could guarantee a transmission success rate of above 85% for both 5G and WiFi most of the time when the experiment was conducted. On the other hand, in the case when no power control is applied (blue curve), the WiFi traffic was completely blocked out during the interval when the AP power is lowered by 10dB. Moreover, the fixed-step power control experiment showed that the 5G UE Rx success rate and the WiFi STA RX success rate suppress each other. They oscillated according to the 5G Tx power level, with an increase in one accompanying a decrease in the other and vice versa.

Finally, we evaluated the energy performance of different power control techniques for both systems in terms of the amount of energy required to transmit one bit successfully, measured in nJ/b. A smaller value indicates better energy performance. The 5G system transmitted 98,560 bits in each time interval, while the Wi-Fi system transmitted 80,008 bits in each time interval. We conducted experiments with different power control methods using the AP power profile in Figure 13 and calculated the average energy performance in nJ/b. Figure 14 shows the energy required by the 5G and Wi-Fi transmitters under different power control methods. We observe that the average energy consumption of the

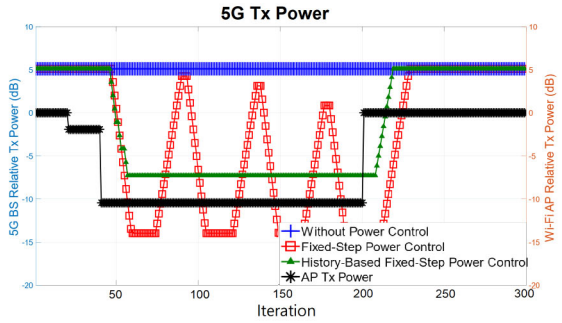

(a) 5G Tx power profile.

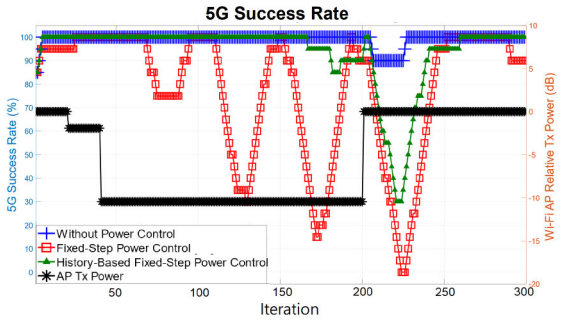

(b) 5G transmission success rate.

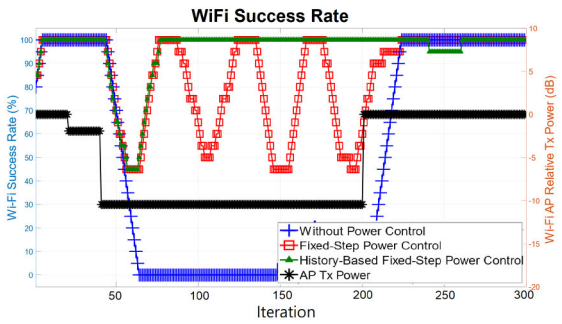

(c) WiFi transmission success rate.

FIGURE 13. Performance comparison of different power control methods: (a) 5G Tx power versus time, (b) 5G success rate versus time, (c) Wi-Fi success rate versus time.

5G BS transmitter was higher than that of the Wi-Fi AP transmitter, mainly because the 5G BS transmitter used an 8-antenna array with beamforming and beam-nulling techniques, while the Wi-Fi AP Tx has only one antenna.

On the 5G side, the required energy depended on the total transmission power and the number of successfully transmitted bits. The proposed method considered the past transmission success rates to avoid a significant 5G Tx power decrease that could decrease the number of successfully transmitted 5G bits. Therefore, it had the best energy performance, i.e., the lowest average energy required per successfully transmitted bit.

On the Wi-Fi side, the proposed power control method also achieved the best energy performance. Since the Wi-Fi AP power profile was fixed, the consumed energy was entirely determined by the number of successfully transmitted bits.

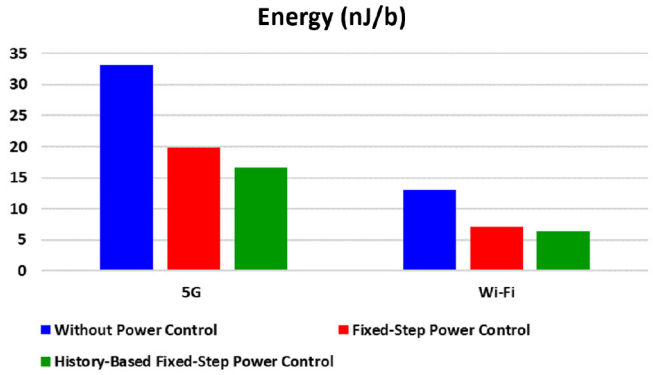

FIGURE 14. Transmission energy of 5G and WiFi transmitters using different power control methods.

The proposed power control method actively adjusted the 5G BS transmission power when the Wi-Fi AP Rx was severely interfered with, thus increasing the number of successfully transmitted WiFi bits and resulting in better energy performance.

To sum up, in the OTA experiments, the history-based fixed-step power control method can improve the measured energy performance of 5G transmission by 50% and Wi-Fi transmission by 51% compared to the case with no power control.

VI. CONCLUSION

This paper proposes a design for 5G BS beamforming transmitter with space-division multiple access and interference avoidance capability. In addition, the BS is capable of tracking the device angles for real-time beamformer adjustment, as well as power control for energy-efficient transmission. To validate the efficiency of the proposed BS design, we employed a cost-effective Xilinx RFSoC evaluation platform for an eight-antenna beamforming transmitter. Another RFSoC platform implemented a four-antenna for monitoring WiFi signal and estimating its arrival angle. These two items of gathered and estimated data are crucial in the proposed device tracking and power control techniques. All other 5G UEs and WiFi AP/STAs are implemented in USRP instruments using software-defined radios.

With the help of the MVDR beamforming technique, the 5G BS prototype can transmit signals to UEs while suppressing the interference level to Wi-Fi STAs. The successful coexistence of 5G and Wi-Fi systems that serve two 5G UEs and two Wi-Fi STAs simultaneously in the same frequency band was demonstrated in the OTA experiment. We also implemented device tracking and power control functions in the 5G BS prototype and conducted another OTA experiment.

The experiments have some limitations and deviate from actual field trials. For instance, we showed only QPSK/16QAM modulations, while the 5G NR standard specifies higher modulation levels. The FEC code rate is set to a low 1/3, while higher code rates are also supported, albeit with degraded reception performance. The demonstration was conducted in a conference room with line-of-sight (LOS) conditions. The TX-RX separation is short due to the lack of power amplifiers in the RFSoC platform.

Despite all the aforementioned limitations, the experiments showcased the effectiveness of the prototype to agilely track the Wi-Fi STA movement and dynamically adjust its transmission power to accommodate WiFi AP Tx power changes. In conclusion, we believe that the proposed 5G BS prototype serves as a successful demonstration of how beamforming, signal angle estimation, and power control can enable the coexistence of 5G and WiFi systems and enhance their transmission reliability and energy performance.

REFERENCES

[1] N. Patriciello, S. Lagen, B. Bojovic, and L. Giupponi, "NR-U and IEEE 802.11 technologies coexistence in unlicensed mmWave spectrum: Models and evaluation," *IEEE Access*, vol. 8, pp. 71254–71271, 2020.

[2] B. Zheng et al., "Design of multi-carrier LBT for LAA and WiFi coexistence in unlicensed spectrum," *IEEE Netw.*, vol. 34, no. 1, pp. 76–83, Jan./Feb. 2020.

[3] *Coexistence Study for LTE-U SDL V1.0*, LTE-U Forum, New York, NY, USA, Feb. 2015.

[4] M. I. Rahman, A. Behravant, H. Koorapaty, J. Sachs, and K. Balachandran, "License-exempt LTE systems for secondary spectrum usage: Scenarios and first assessment," in *Proc. IEEE Symp. New Front. Dyn. Spectr. Access Netw.*, 2011, pp. 349–358.

[5] *LTE in Unlicensed Spectrum: Harmonious Coexistence With Wi-Fi*, Qualcomm Res., San Diego, CA, USA, Jun. 2014.

[6] Q. Ren, J. Zheng, B. Wang, and Y. Zhang, "Performance modeling of an NR-U and WiFi coexistence system with NR-U type B multichannel access procedure," *IEEE Internet Things J.*, vol. 10, no. 5, pp. 4403–4419, Mar. 2023.

[7] M. Haghshenas and M. Magarini, "NR-U and Wi-Fi coexistence enhancement exploiting multiple bandwidth parts assignment," in *Proc. IEEE 19th Annu. Consum. Commun. Netw. Conf. (CCNC)*, Las Vegas, NV, USA, 2022, pp. 260–263.

[8] T G. Geraci, A. Garcia-Rodriguez, D. López-Pérez, A. Bonfante, L. G. Giordano, and H. Claussen, "Operating massive MIMO in unlicensed bands for enhanced coexistence and spatial reuse," *IEEE J. Sel. Areas Commun.*, vol. 35, no. 6, pp. 1282–1293, Jun. 2017.

[9] A. Zubow, P. Gawowicz, and S. Bayhan, "XZero: On practical cross-technology interference-nulling for LTE-U/WiFi coexistence," 2018, *arXiv:1801.07992*.

[10] L. Bertizzolo, E. Demirors, Z. Guan, and T. Melodia, "CoBeam: Beamforming-based spectrum sharing with zero cross-technology signaling for 5G wireless networks," in *Proc. IEEE INFOCOM Conf. Comput. Commun.*, Toronto, ON, Canada, 2020, pp. 1429–1438.

[11] L. Wang et al., "Spatial-reuse-based efficient coexistence for cellular and WiFi systems in the unlicensed band," *IEEE Internet Things J.*, vol. 9, no. 3, pp. 1885–1898, Feb. 2022.

[12] P. Li and D. Liu, "Efficient beam selection and resource allocation scheme for WiFi and 5G coexistence at unlicensed millimeter-wave bands," *IET Commun.*, vol. 14, no. 17, pp. 2944–2952, Oct. 2020.

[13] H. L. Van Trees, *Optimum Array Processing (Detection, Estimation, and Modulation Theory, Part IV*. Hoboken, NJ, USA: Wiley, 2002.

[14] J. H. Chang, L. Tassiulas, and F. Rashid-Farrokhi, "Joint transmitter receiver diversity for efficient space division multiaccess," *IEEE Trans. Wireless Commun.*, vol. 1, no. 1, pp. 16–27, Jan. 2002.

[15] Z. Guo, M. Li, and M. Krunz, "Exploiting successive interference cancellation for spectrum sharing over unlicensed bands," *IEEE Trans. Mobile Comput.*, vol. 23, no. 3, pp. 2438–2455, Mar. 2004.

[16] T. Y. Wang and T. D. Chiueh, "Design and implementation of time-domain interference cancellation receiver for LTE-U systems," *IEEE Access*, vol. 8, pp. 156986–156995, 2020.

[17] M. M. Elahi, K. J. Valdez, and V. Gonzalez, "LTE/Wi-Fi coexistence on a flexible software defined radio testbed," in *Proc. Int. Found. Telemetering*, 2022, pp. 1–9.

[18] M. Zając and S. Szott, "Resolving 5G NR-U contention for gap-based channel access in shared sub-7 GHz bands," *IEEE Access*, vol. 10, pp. 4031–4047, 2022.
[19] K. Kosek-Szott et al., "Downlink channel access performance of NR-U: Impact of numerology and mini-slots on coexistence with Wi-Fi in the 5 GHz band," *Comput. Netw.*, vol. 195, Jan. 2021, Art. no. 108188.
[20] S. Malkowsky et al., "The world's first real-time testbed for massive MIMO: Design, implementation, and validation," *IEEE Access*, vol. 5, pp. 9073–9088, 2017.
[21] P. Harris et al., "LOS throughput measurements in real-time with a 128-antenna massive MIMO testbed," in *Proc. IEEE Global Commun. Conf. (GLOBECOM)*, Washington, DC, USA, Dec. 2016, pp. 1–7.
[22] X. Yang et al., "Design and implementation of a TDD-based 128-antenna massive MIMO prototype system," *China Commun.*, vol. 14, no. 12, pp. 162–187, Dec. 2017.
[23] "MUSIC (Algorithm)." Accessed: Apr. 1, 2023. [Online]. Available: https://en.wikipedia.org/wiki/MUSIC_(algorithm)
[24] A. Zahernia, M. J. Dehghani, and R. Javidan, "MUSIC algorithm for DOA estimation using MIMO arrays," in *Proc. Int. Conf. Telecommun. Syst. Services Appl. (TSSA)*, Denpasar, Indonesia, 2011, pp. 149–153.
[25] C. W. Sung and W. S. Wong, "A distributed fixed-step power control algorithm with quantization and active link quality protection," *IEEE Trans. Veh. Technol.*, vol. 48, no. 2, pp. 553–562, Mar. 1999, doi: 10.1109/25.752580.
[26] 3GPP. "5G NR multiplexing and channel coding." 2020. Accessed Sep. 3, 2022. [Online]. Available: https://www.etsi.org/deliver/etsi_ts/138200_138299/138212/15.09.00_60/ts_138212v150900p.pdf
[27] H. M. Ji and E. Killian, "Fast parallel CRC algorithm and implementation on a configurable processor," in *Proc. IEEE Int. Conf. Commun.*, vol. 3. New York, NY, USA, 2002, pp. 1813–1817.
[28] *5G NR Physical Channels and Modulation*, 3GPP Standard TS 38.211, 2020. Accessed: Sep. 3, 2022. [Online]. Available: https://www.etsi.org/deliver/etsi_ts/138200_138299/138211/15.08.00_60/ts_138 211v150800p.pdf
[29] Xilinx. "Soft-decision FEC integrated block." Accessed: Apr. 1, 2023. [Online]. Available: https://www.xilinx.com/products/intellectual-property/sd-fec.html

YU-HAO LIU was born in Taiwan. He received the B.S. degree in electrical and computer engineering from National Chiao Tung University in 2020 and the M.S. degree in electronics engineering from National Taiwan University in 2022. He is currently with Mediatek, Inc. His research interest includes coexistence beamforming systems and software-defined radio systems.

CHENG-BANG KU was born in Taiwan. He received the B.S. degree in electrical engineering from National Tsing Hua University in 2020. He is currently pursuing the M.S. degree in electronics engineering with National Taiwan University. His research interest includes wireless communication and digital circuit design.

TZI-DAR CHIUEH (Fellow, IEEE) was born in Taipei, Taiwan, in 1960. He received the B.S.E.E. degree from National Taiwan University, Taipei, Taiwan, in 1983 and the M.S. and Ph.D. degrees in electrical engineering from the California Institute of Technology, Pasadena, California, in 1986 and 1989, respectively.

Since 1989, he has been with the Department of Electrical Engineering, National Taiwan University, where he is presently a Distinguished Professor, the Dean of the Graduate School of Advanced Technology, and he served as the Director of the Graduate Institute of Electronics Engineering from 2004 to 2007. He has held visiting positions with ETH Zurich, Switzerland, from 2000 to 2001 and the State University of New York at Stony Brook from 2003 to 2004. His research interests include IC design for digital communication systems, neural network, and signal processing for bio-medical systems.

Prof. Chiueh's teaching efforts were recognized 11 times by the Teaching Excellence Award from NTU. He was the recipient of the Outstanding Research Award from National Science Council, Taiwan, from 2004 to 2007. In 2005, he received the Outstanding Electrical Engineering Professor from the Chinese Institute of Electrical Engineers Taiwan, and was awarded the Himax Chair Professorship with National Taiwan University in 2006. In 2009, he received the Outstanding Industry Contribution Award from the Ministry of Economic Affairs, Taiwan. He received the Outstanding Technology Transfer Contribution Award from Ministry of Science and Technology, Taiwan, in 2016. From November 2010 to January 2014, he served as the Director General for the National Chip Implementation Center Hsinchu, Taiwan. He also served as the Vice President for the National Applied Research Laboratories from 2015 to 2017. He is the NTU Macronix Chair Professor in 2021.